The Journal of Neuroscience, November 1994, 14(11): 6392–6401

Regional Modulation of Neurofilament Organization by Myelination in Normal Axons

Sung-Tsang Hsieh,[1,5] Grahame J. Kidd,[2] Thomas O. Crawford,[2,4] Zuoshang Xu,[3] Whei-Min Lin,[2] Bruce D. Trapp,[2] Don W. Cleveland,[1,3] and John W. Griffin[1,2]

Departments of [1]Neuroscience, [2]Neurology, [3]Biological Chemistry, and [4]Pediatrics, The Johns Hopkins University School of Medicine, Baltimore, Maryland 21287 and [5]Department of Neurology, National Taiwan University Hospital, Taipei, Taiwan, Republic of China

Previous studies in the hypomyelinating mouse mutant *Trembler* have suggested that demyelinating axons are smaller in caliber compared to normal axons, and that there are differences in the organization of axonal neurofilaments. In the normal PNS, however, the relationship between neurofilament organization and myelination has not been investigated extensively. In normal axons, only the initial segments, the nodes of Ranvier (~1 μm), and the terminals are not covered by myelin. We took advantage of an unusual feature of the primary sensory neurons in the dorsal root ganglion, the relatively long nonmyelinated stem process (up to several hundred micrometers), to determine if the presence of myelination correlates with differences in cytoskeletal organization and neurofilament phosphorylation. Axonal caliber and neurofilament numbers were substantially greater in the myelinated internodes than in the stem process or nodes of Ranvier. Neurofilament spacing, assessed by measuring the nearest-neighbor neurofilament distance, was 25–50% less in the stem processes and nodes of Ranvier than in the myelinated internodes. In the myelinated internodes, neurofilaments had greater immunoreactivity for phosphorylated epitopes than those in the stem process. These findings indicate that interactions with Schwann cells modulate neurofilament phosphorylation within the ensheathed axonal segments, and that increased phosphorylation within myelinated internodes leads to greater interfilament spacing. Lastly, the myelinated internodes had three fold more neurofilaments, but the same number of microtubules. Both the increased neurofilament spacing and the increase in neurofilament numbers in myelinated internodes contribute to a greater axonal caliber in the myelinated internodes.

[Key words: neurofilament phosphorylation, nearest-neighbor distance, myelination, Schwann cell, dorsal root ganglion, initial segment, stem process, node of Ranvier, axonal caliber, morphometry]

In large neurons neurofilaments are the most abundant cytoskeletal organelles, and have been postulated to act as important intrinsic determinants of axonal caliber (Hoffman et al., 1987). Neurofilaments in vertebrates are composed of three related proteins with apparent molecular weights of 68, 150, 200 kDa (NF-L, NF-M, and NF-H, respectively) (Hoffman and Lasek, 1975; Liem et al., 1978; Geisler et al., 1983; Willard and Simon, 1983; Hirokawa et al., 1984; Schlaepfer, 1987). All three of these proteins share a central rod domain, but they differ in their C-terminal regions. In NF-H, this region contains over 40 lysine-serine-proline repeats (Julien et al., 1986, 1988; Lees et al., 1988), which provide potential phosphorylation sites (Julien et al., 1983; Geisler et al., 1983; Lee et al., 1988). The extent of phosphorylation of this region, which contributes to the side-arms of the neurofilament (Hirokawa et al., 1984; Carden et al., 1985; Hisanaga and Hirokawa, 1988), appears to differ within different regions of the neuron, with a higher phosphorylation state in the axon than in the cell body and dendrite (Sternberger and Sternberger, 1983; Lee et al., 1986, 1987). One attractive hypothesis is that phosphorylation on the side arms may increase spacings between nearest-neighbor neurofilaments (Carden et al., 1987), and thereby achieve a larger axonal caliber.

Axonal caliber is a fundamental phenotypic feature of neurons. For each of the different functional classes of peripheral nerve fibers, there is a restricted range of normal axonal calibers. The conduction velocity of nerve action potential is a function of fiber diameter (for review, see Waxman, 1980). Axonal caliber is considered to be largely determined developmentally. A special role of neurofilaments in influencing caliber has been deduced from the observation that neurofilament density is relatively constant among axons of different calibers (Friede and Somarajski, 1970; Hoffman et al., 1984), although regional differences (Nixon and Logvinenko, 1986; Lasek, 1988; Price et al, 1990; Reles and Friede, 1991), changes in axonal diseases (Parhad et al., 1987; Dyck et al., 1990), and alterations due to interrupted axon–target interactions (Hoffman et al., 1984) all indicate that neither neurofilament number nor density is fixed or immutable.

Few studies have examined the possible effects of ensheathing cells or myelination on the axon or its cytoskeleton (Aguayo et al., 1977; Windebank et al., 1985; de Waegh et al., 1992). In the PNS, all axons are ensheathed by Schwann cells. Schwann cells elaborate specialized lamellated plasmalemma sheaths, the myelin sheaths, around some of the PNS axons. These myelin sheaths are interrupted periodically at the nodes of Ranvier. Myelination is associated with increased axonal caliber in mye-

Received Aug. 27, 1993; revised Mar. 11, 1994; accepted Mar. 29, 1994.

This work was supported by NIH Grants to J.W.G. (NINDS Grant RO1-14784); to J.W.G., D.W.C., and B.D.T. (NS PO1-22849), to S.-T.H. (NIMH Grant 5T32 MH 18030); and to T.O.C. (NINDS CIDA NS 01412). We thank Eileen Mulrenin and Carol Haney for technical assistance; Drs. Paul Hoffman, Michael Shelanski, and Phil Wong for suggestions and discussion, and Rod Graham for editorial assistance. G.J.K. and Z.X. are postdoctoral fellows of the National Multiple Sclerosis Society, and the Muscular Dystrophy Association, respectively.

Correspondence should be addressed to Dr. John W. Griffin, Johns Hopkins Hospital, Department of Neurology, Meyer 6-109, 600 North Wolfe Street, Baltimore, MD 21287-7609.

linating tissue culture (Windebank et al., 1985), and the nodes of Ranvier are smaller than the neighboring myelinated internodes (Berthold, 1978). From these observations, it has been presumed that myelination has some effect on the axonal cytoskeleton. In a series of studies by nerve-graft experiments, de Waegh and colleagues provided a possible basis for this effect in studies of the hypomyelinating/demyelinating mouse mutant, *Trembler* (de Waegh and Brady, 1990, 1991; de Waegh et al., 1992). Compared to normally myelinated internodes, the *Trembler* internodes were smaller, had closer neurofilament spacing, and had lower levels of phosphorylated NF-H. Based on these observations, de Waegh et al. (1992) proposed that the regional variations in neurofilament organization is modulated by myelinating Schwann cells.

The effect of myelination on the regional variations of axonal cytoskeleton in the normal PNS has not been examined comprehensively. In most large axons, only the short initial segments and the nodes of Ranvier (~1 μm) are not covered by myelin. In this study, we have taken advantage of an unusual feature of the large primary sensory neurons in the dorsal root ganglion (DRG) and trigeminal ganglion, the nonmyelinated axonal stem process, which is usually of tens of micrometers in length (Fig. 1*A*). We asked whether the stem process differed from the myelinated internodes in terms of axonal size, cytoskeletal composition, neurofilament spacing, and the level of neurofilament phosphorylation. The results indicate that those regions covered by myelin are different in all of these features of the axonal cytoskeleton, and are consistent with the hypothesis that myelinating Schwann cells exert a major extrinsic influence on the organization of the axon.

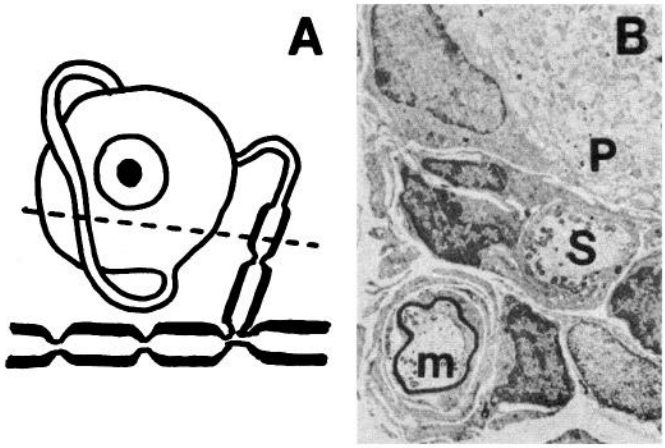

Figure 1. The diagram of a dorsal root ganglion (DRG) neuron. The stem process, the nonmyelinated axonal portion, extends from the cell body to the first internode. If a cross section was made through the *dashed line* of the schematic DRG neuron (*A*), the perikaryon (*p*), stem process (*s*), and the myelinated internodes (*m*) would appear on the same section, as illustrated in the electron micrograph in *B*. The stem process was covered by satellite cells, which did not make myelin sheaths.

Materials and Methods

Tissue preparation: primary sensory ganglion neurons

We studied the primary sensory neurons and their axons in the rat lumbar dorsal root ganglia, and trigeminal ganglion. The stem process, the nonmyelinated portion of the axon that extends from the cell body of the sensory neurons to the first myelin heminode (Spencer et al., 1973), varies in its length and course. Long stem processes wrap around their cell bodies in a glomerular fashion. On cross sections, the stem process was easily recognized as a nonmyelinated axon lying near the cell body and surrounded by satellite cells (Fig. 1*B*); in neurons with glomerular arrangement the stem process could be seen more than once in a single cross section.

Groups of Sprague–Dawley rats (8–12 weeks of age, with body weights of 200–300 gm) and C57 mice (6–8 weeks of age) were anesthetized with 4% chloral hydrate and animals were fixed by intracardiac perfusion with 4% paraformaldehyde/3% glutaraldehyde (for ultrastructural morphometry), 4% paraformaldehyde (for light microscopic immunocytochemistry), or 4% paraformaldehyde/0.5% glutaraldehyde (for electron microscopic immunocytochemistry) in 0.1 M Sorenson's phosphate buffer. The lumbar DRGs and trigeminal ganglia with roots attached were dissected out and postfixed in the same fixatives for another 24 hr, and then transferred to buffers.

Ultrastructural morphometry

Preparations. The lumbar DRGs and dorsal roots were postfixed in 2% osmium tetroxide, embedded in Epon and sectioned in an ultramicrotome. Relatively thick thin-sections (silver-gold to gold reflection) were picked up on Formvar-coated grids, stained with uranyl acetate and lead citrate, and observed under electron microscope. Individual stem processes were identified and photographed at 10,000× and 40,000×. For each stem process the adjacent myelinated axon and the nerve cell body were photographed at the same magnifications.

To compare the cytoskeletal organization between the node of Ranvier and the internode of the same axon, serial thin sections intermixed with thick sections of the dorsal roots (total of 300 thin sections and 20 thick sections) were cut. The criteria of defining a node of Ranvier included (1) the absence of myelin, (2) the presence of Schwann cell microvilli, and (3) the presence of dense undercoatings on axonal membrane. When a node of Ranvier was identified, we traced forward and backward to find its corresponding internode and photographed both sites at 6000×, 10,000×, and 40,000×.

Cytoskeletal composition. To estimate the cytoskeletal composition, we modified the previous method of Parhad et al. (1987). Briefly, we divided the whole cross-section axonal area into tiles of 1 μm^2, assigned consecutive numbers (beginning from 1) on each tile, chose one to five tiles based on the numbers of a random table, and counted the whole axonal neurofilament densities (expressed as neurofilaments/μm^2 axonal area) on those selected squares. The mean of the whole axonal neurofilament densities for each sampled axon was multiplied by the axonal area to give the estimated total number of neurofilaments for that axon. The same procedure was repeated for the estimation of the total number of microtubules per axon. For stem process and node of Ranvier, one to five 1 μm^2 tiles constituted 50–90% of axonal area. For myelinated axons, the sampled regions would be responsible for 16–40% of axonal area. In the myelinated axons, the region occupied by membrane-bound organelles (mitochondria, smooth endoplasmic reticulum, and vesicular organelles) was negligible (less than 5% of axonal area) (Berthold, 1978; Hoffman et al., 1984). In the stem process and nodes particulate organelles occupied a greater area of the cross-sectional area, so that the whole axonal density data cannot be used for comparing neurofilament spacing. Price et al. (1990) and de Waegh et al. (1992) calculated neurofilament packing density by excluding the area occupied by particulate organelles. In this study, we used nearest-neighbor distance to compare neurofilament spacing (see below); the whole axonal density data were used to calculate the total number of neurofilaments and microtubules.

Nearest-neighbor distance. We used the analysis of nearest-neighbor distance to measure neurofilament spacing. The nearest-neighbor distance approach identifies obligate minimum spacing and the degree of variations in spacing of neurofilaments. Both nearest-neighbor distance and packing density are complementary and necessary to understand neurofilament organization and distribution (Hsieh et al., 1994). Briefly, the negatives of electron micrographs were illuminated on a view box, imaged with a video camera. Each neurofilament that was oriented in true transverse section was accepted and digitized with the BIOQUANT software (R&M Biometrics, Inc., Nashville, TN). The data of x-y ordinates for each neurofilament were exported to a database. A program was written to calculate the nearest-neighbor distance for each neurofilament. In addition, axonal area, axonal circumference, and myelin sheath thickness were measured with the BIOQUANT software to compare their relationships with neurofilament spacing.

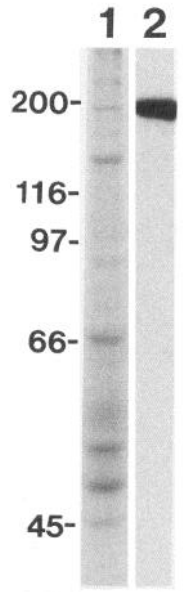

Figure 2. Immunoblotting to characterize the polyclonal antibody pAb-NFH. The antibody pAb-NFH was made against the C-terminus of NF-H. Protein extract of mouse spinal cord was electrophoresed on 7% SDS-polyacrylamide gel and stained with Coomassie blue (*lane 1*). A duplicate gel was transferred onto a nitrocellulose paper (*lane 2*). Immunoblotting in *lane 2* indicated that pAb-NFH recognized NF-H as a discrete band.

Antibodies against different epitopes of neurofilament proteins

We used immunoreactivity against different epitopes of NF-H (phosphorylated, nonphosphorylated and phosphorylation-independent epitopes) to assess the regional difference of neurofilament phosphorylation. SMI-31 and SMI-32 are mouse monoclonal antibodies (Sternberger Monoclonals Inc., Baltimore, MD). They have been characterized in terms of their phosphorylation status. SMI-31 is directed against the extensively phosphorylated form of NF-H, the sequence motif containing highly phosphorylated lysine-serine-proline. The SMI-32 recognize a nonphosphorylated or relatively hypophosphorylated form of this motif on neurofilaments (Sternberger and Sternberger, 1983; Lee et al., 1988).

For the purpose of recognizing all the NF-H, independent of phosphorylation state, a polyclonal antibody (termed pAb-NFH in this report) was made against NF-H. The peptide CYEKTTEDKATKGEK (one-letter code for amino acid), which corresponds to the carboxyl terminal 13 amino acids of mouse NF-H (Julien et al., 1986; Julien et al., 1988) plus C and Y at its N-terminus for coupling and UV detection, was chemically synthesized using a peptide synthesizer. The peptide was then coupled to keyhole limpet hemocyanin and used to immunize rabbits. Purification of the antibody was carried out as described previously (Lopata and Cleveland, 1987).

To characterize the antibody pAb-NFH, approximately 20 μg of total protein extract from mouse spinal cord was electrophoresed on a 7% SDS-polyacrylamide gel (Laemmli, 1970), and stained with Coomassie blue. A duplicate gel was transferred onto a nitrocellulose filter as described before (Lopata and Cleveland, 1987). The nitrocellulose filter was then incubated with the purified antibody pAb-NFH in 2% powder milk and PBS for 2 hr. After the filter was washed five times with PBS, it was incubated with ^{125}I-protein A (Amersham Corp., Arlington Heights, IL) for 1 hr. The filter was then repeatedly washed and exposed to x-ray film. On immunoblotting, pAb-NFH recognized neurofilaments as a band at the 200 kDa position on immunoblotting (Fig. 2). Because there are no potential serine phosphorylation sites in this region of the carboxy terminus of NF-H (Julien and Mushynski, 1983; Julien et al., 1986, 1988), pAb-NFH should recognize the total NF-H independent of phosphorylation status.

Immunocytochemistry and confocal laser scanning microscopy

The dissected rat lumbar DRGs, rat, and mouse trigeminal ganglia were cryoprotected with 20% glycerol in the Sorenson's buffer for 24 hr and then cut on a freezing microtome. Sections of 20–30 μm thickness were rinsed in PBS solution, incubated with 25% Triton X-100 in PBS for 24 hr to increase antibody penetration, and then blocked with 5% normal horse serum for 30 min. Tissue sections were labelled by incubating them in a combination of mouse and rabbit antibodies in 1% Triton X-100/PBS at 4°C for 24 hr. The primary antibodies used in this study included the monoclonal antibodies against phosphorylated neurofilaments (SMI-31) and nonphosphorylated neurofilaments (SMI-32), and a polyclonal antibody against myelin protein P_0 (Trapp et al., 1981). The sections were washed and then incubated in a mixture of fluorescein isothiocyanate (FITC)-conjugated sheep anti-mouse and Texas red–conjugated donkey anti-rabbit antibodies (Amersham Corp., Arlington Heights, IL) for 2 hr. The sections were washed in PBS and mounted in a fade-resisting mowiol-based mounting medium containing paraphenylene diamine.

The sections were examined with standard epifluorescence and imaged with a Leica confocal laser scanning microscope. Optical sections of approximately 0.5–1 μm thick were collected using a line averaging technique. The Texas red and FITC images were collected simultaneously. In some cases, serial sequences of optical sections were obtained at 1–2 μm intervals through the profiles. The continuity and staining patterns of myelinated and non-myelinated portions of the same axon were investigated using these "z-series" either viewed as a sequence of single images or in three-dimensional reconstructions and rotations.

Electron microscopic immunocytochemistry

The procedure of electron microscopic immunocytochemistry followed that previously reported (Trapp et al., 1989). Briefly, the rat lumbar DRGs were infiltrated with 1 M, 2 M, and 2.3 M sucrose solution containing 30% polyvinylpyrrolidone. Frozen sections were cut on a Reichert ultramicrotome in a liquid nitrogen–cooled chamber (around −100°C). Thin sections around 100 nm in thickness were picked up on Formvar-coated grids, rinsed with PBS, blocked with ovalbumin/normal goat serum, and incubated with primary antibodies (SMI-31 and pAb-NFH) for 16–24 hr. After washing in PBS, grids were incubated with 10 nm colloidal gold-labeled goat anti-mouse IgG (for SMI-31) and 5 nm colloidal gold-labeled goat anti-rabbit IgG (for pAb-NFH) for 2 hr. The sections were fixed with glutaraldehyde, stained with uranyl acetate, embedded in uranyl acetate-containing methyl cellulose, and observed under a Hitachi 600 electron microscope.

To assess the relative intensity of labeling, stem processes and myelinated axons on the grids were photographed at 60,000×. The densities of immunogold particles in the axons were measured using BIOQUANT software.

Statistical analysis

T test, Wilcoxon ranked sums test, and regression statistics were generated by using the STATISTICAL ANALYSIS SYSTEM program (SAS Institute Inc., Cary, NC). Differences with $p < 0.05$ were considered statistically significant.

Results

Axonal caliber and cytoskeletal composition in myelinated and nonmyelinated segments

To test whether variations of axonal caliber and cytoskeletal composition were related to the myelination status of the axonal segment, we sampled eight stem processes and nine neighboring myelinated axons and compared the following parameters: axonal caliber, and the total number of neurofilaments, and microtubules per axon. Myelinated axons were larger than stem processes [axonal area: 26.3 ± 9.4 vs 11.0 ± 4.8 μm^2 (mean ± SD), $p < 0.01$]. Ultrastructurally, neurofilaments appeared as 10 nm electron-dense dots in axonal cross section and had side arms extending as thin threads from the core of neurofilaments. The most impressive feature of the cytoskeleton in the stem process was the greater proportion of microtubules, and other membrane-bound organelles and the smaller proportion of neurofilaments compared to the pattern in the myelinated segments (Fig. 3; Berthold, 1978). Compared to the stem process, the myelinated internodes had threefold more neurofilaments (6760

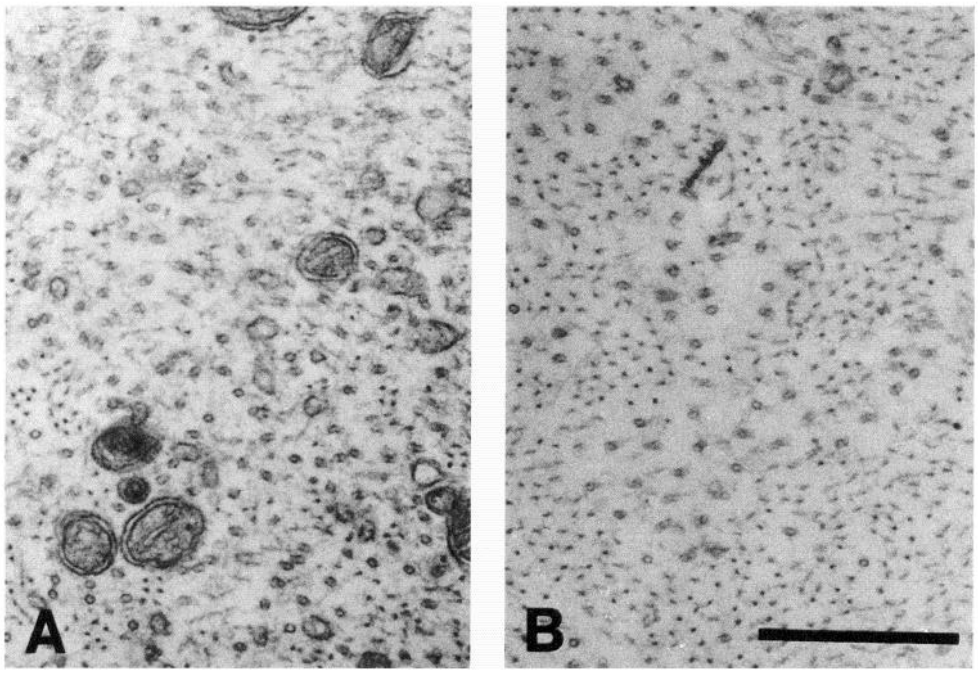

Figure 3. Regional differences in axonal cytoskeleton between the stem process and myelinated axon. Representative sections were taken from a stem process (*A*) and a myelinated internode (*B*). Compared with the myelinated internode, the stem process had fewer neurofilaments, denser microtubules, mitochondrial and vesicular organelles. Neurofilaments in the stem process tended in cluster. Scale bar, 0.5 μm.

± 2,427 vs 2423 ± 1474 neurofilaments per axon, $p < 0.01$), but similar numbers of microtubules (614 ± 423 vs 538 ± 188 microtubules per axon, $p = 0.73$).

To analyze further the correlation of myelination with the regional differences in cytoskeletal composition, we traced individual axons in the rat dorsal roots and analyzed morphometrically six node of Ranvier/internode pairs in six axons. The results were similar to the stem process/internode comparison (Fig. 4). Compared to the nodes of Ranvier, the myelinated internodes were larger in axonal area (29.5 ± 8.9 vs 4.1 ± 1.7 μm^2, $p < 0.01$), had a greater number of neurofilaments (6505 ± 2025 vs 879 ± 627 neurofilaments per axon, $p < 0.01$), and had the same total number of microtubules (499 ± 197 vs 578 ± 171 microtubules per axon, $p = 0.47$).

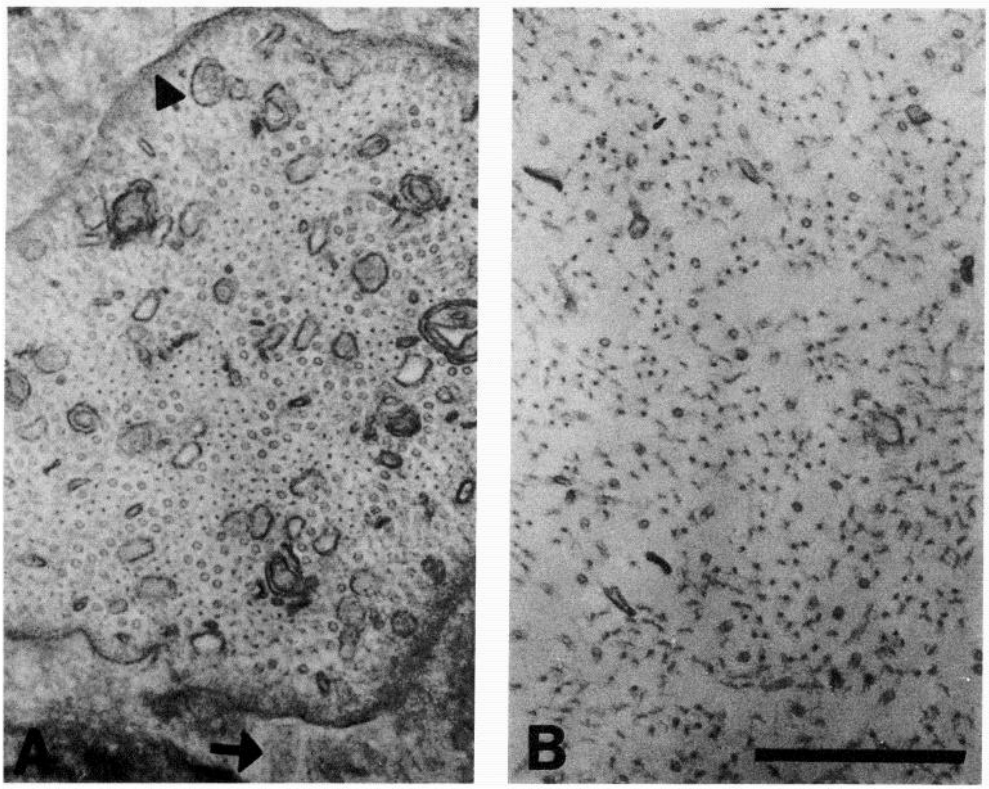

Figure 4. The comparison of cytoskeletal composition between the node of Ranvier and its internode. The node of Ranvier (*A*) was recognized by its absence of myelin sheath, and its presence of Schwann cell microvilli (*arrow*) and the dense undercoatings on axonal membrane (*arrowhead*). The node of Ranvier had less neurofilaments and denser microtubules and vesicular organelles than its myelinated internode (*B*). Scale bar, 0.5 μm.

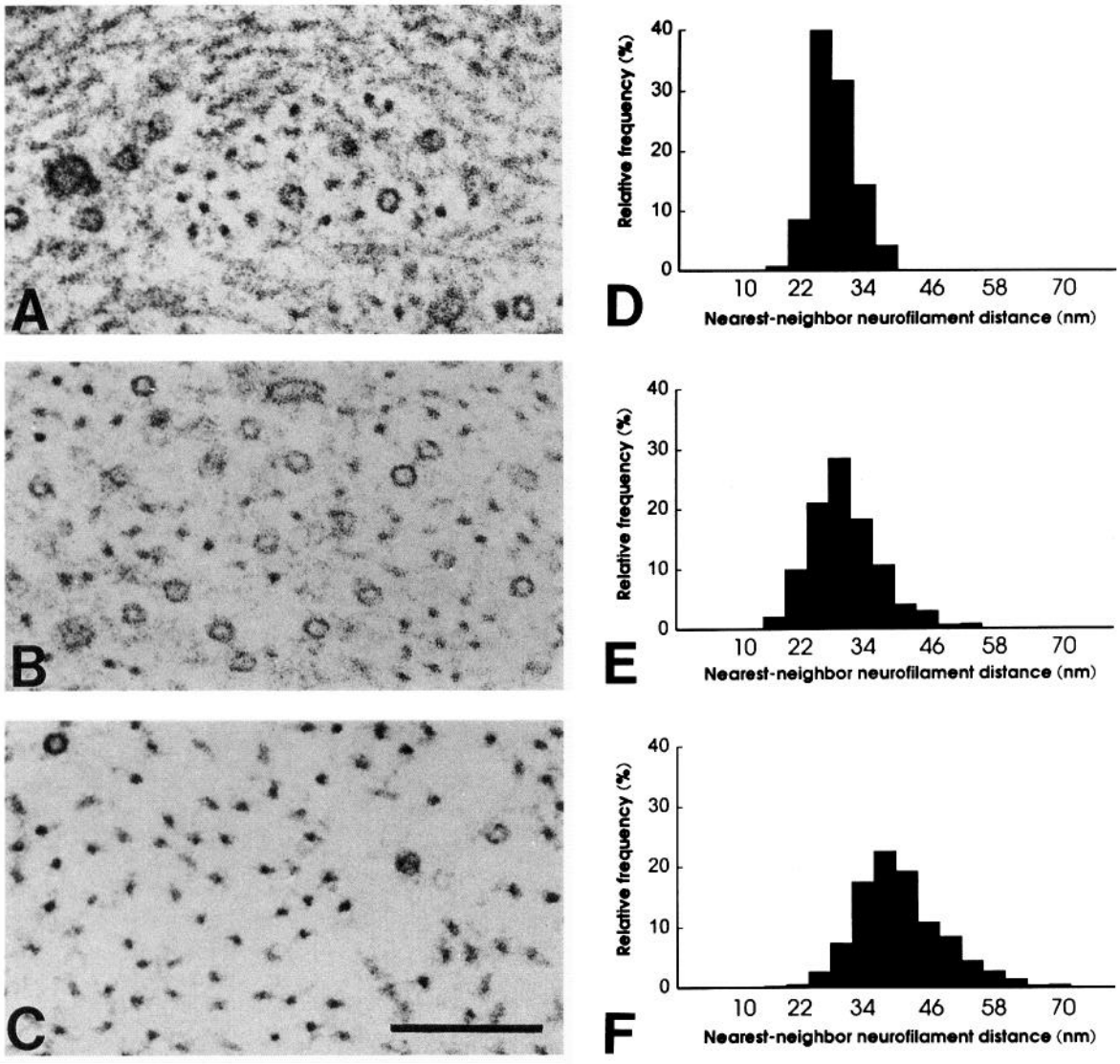

Figure 5. Neurofilament distribution in different regions of dorsal root ganglion (DRG) neurons. Neurofilaments tend to be in different orientations in the cell body of DRG neurons (*A*). Occasionally bundles of neurofilaments in cross section can be found. In the stem process (*B*), neurofilaments were sometimes clustered between microtubules. In the myelinated axon (*C*), neurofilaments were more widely spaced in the stem process. The corresponding histograms of nearest-neighbor neurofilament distances were shown in the *right panels*. Neurofilaments in the cell bodies and the stem processes had spacings of 28.9 ± 4.4 and 32.2 ± 7.7 nm (mean ± SD), respectively (*D* and *E*), which were ~25–30% smaller than in the myelinated axons (*F*) (40.3 ± 9.3 nm; $p < 0.001$ by *t* test). The comparison was based on six DRG neurons (with 390 digitized neurofilaments), nine stem processes (with 4634 digitized neurofilaments), and 15 myelinated axons (with 20,301 digitized neurofilaments). Scale bar, 200 nm.

The regional increase in neurofilament spacing correlates with myelination

To correlate myelination with regional differences in neurofilament spacing, we compared nearest-neighbor neurofilament distances in the cell bodies, the nonmyelinated stem process and myelinated axons. In the perikaryon, neurofilaments tended to be in different orientations, and occasionally in bundles (Fig. 5*A*). In the stem process (Fig. 5*B*), neurofilaments were not only fewer in number, but were also more closely packed than in the myelinated internodes (Fig. 5*C*). Neurofilaments in the cell body and stem process sometimes appeared as clusters interspersed among the microtubules. Neurofilaments were not clustered through the axoplasm of myelinated internodes. The mean filament–filament spacings in the cell bodies and stem processes were 28.9 ± 4.4 and 32.2 ± 7.7 nm (mean ± SD) (Fig. 5 *D,E*). In myelinated internodes, these values were 25–30% greater than in the perikarya and stem processes: 40.3 ± 9.3 nm ($p < 0.001$) (Fig. 5*F*).

Comparing neurofilament spacing between the nodes and internodes, we found that neurofilaments were sometimes clustered between microtubules in the nodes (Fig. 6*A*), recapitulating the picture seen in the stem process. Neurofilaments in the internodes were more widely spaced (Fig. 6*B*); the nearest-neighbor distances in the nodes of Ranvier were less than in the adjacent internodes [29.2 ± 5.5 vs 44.8 ± 8.6 nm (mean ± SD), $p < 0.001$] (Fig. 6*C*).

We separately compared the relationships among spacing, myelin sheath thickness, and axonal caliber. Fifty-nine axons were analyzed for this purpose, including 10 stem processes (with 5049 neurofilaments sampled) and 49 myelinated axons (with 40,927 neurofilaments sampled). In general, larger fibers

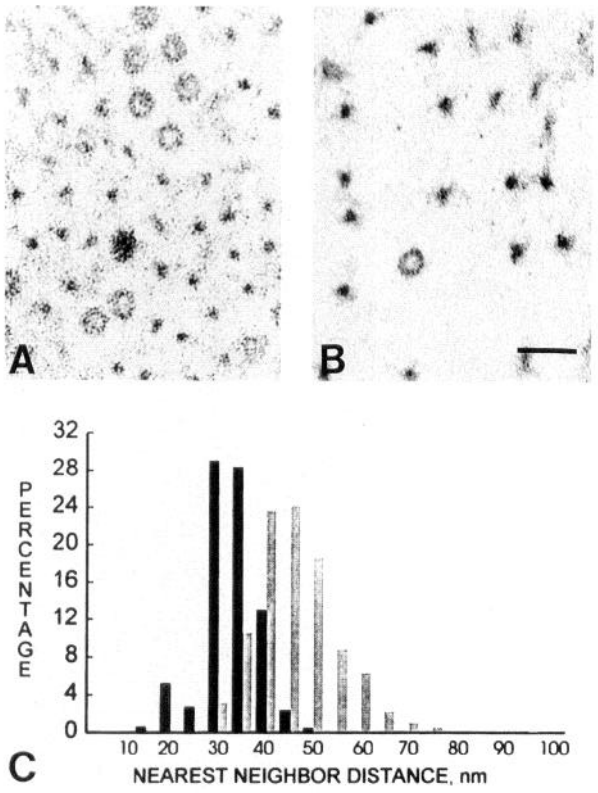

Figure 6. Neurofilament distribution in the node of Ranvier and the adjacent internode. Neurofilaments in node of Ranvier (*A*) were more closely packed than in the adjacent internode (*B*) of the same fiber. In *C*, the comparison of histograms of nearest-neighbor neurofilament distance in nodes of Ranvier (*solid bars*) and internodes (*shaded bars*) indicated that neurofilaments (3156 from six nodes, and 4197 from six internodes) were more closely packed in the nodes [29.2 ± 5.5 vs 44.8 ± 8.6 nm (mean ± SD), $p < 0.001$ by t test]. Scale bar, 50 nm.

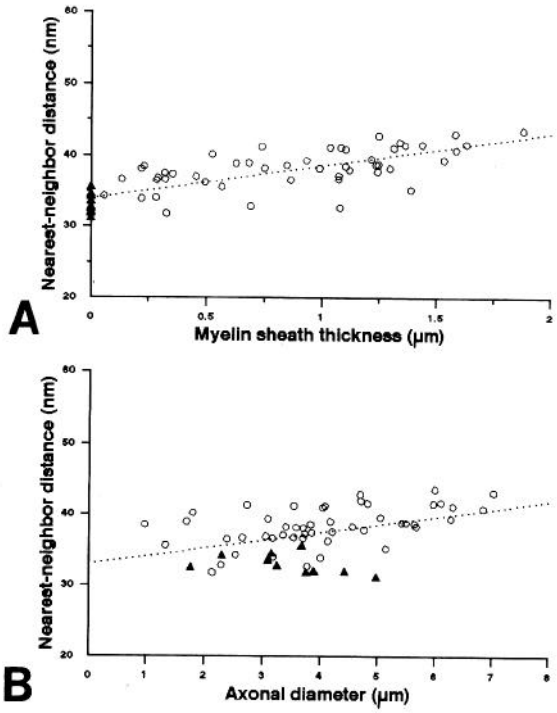

Figure 7. Relationship between mean nearest-neighbor filament spacings, myelin sheath thickness, and axonal diameter. In both *A* and *B*, *open circles* were for myelinated axons, and *solid triangles*, for stem processes. *A*, When the mean of filament spacing (*y-axis*, in nm) was regressed against the myelin sheath thickness (*x-axis*, in μm), the relationship was described by $y = 33.96 + 4.57x$ with correlation coefficient $r = 0.76$, $p < 0.0001$. *B*, The mean filament spacing (*y-axis*, in nm) regressed against the axonal diameter (*x-axis*, in μm) was described by $y = 32.54 + 1.18x$ with correlation coefficient $r = 0.5$, $p < 0.0001$. Myelin sheath thickness correlated better with mean filament spacings than did axonal diameter.

had greater interfilament spacing. The correlation was higher between the mean filament spacing and myelin sheath thickness (Fig. 7*A*) than between the mean filament spacing and axonal caliber (Fig. 7*B*).

Myelination correlates with the regional differences in neurofilament phosphorylation

By using confocal laser scanning microscopy to follow and reconstruct the stem process, and by using double immunofluorescence staining, we found a close relationship between myelination and neurofilament phosphorylation. In the cell bodies, there was strong immunoreactivity for relatively hypo- and nonphosphorylated neurofilament, SMI-32 (Fig. 8*A*). The immunoreactivity for extensively phosphorylated neurofilament antibody, SMI-31, was much weaker in the cell body than in the myelinated axons (Fig. 9*A*). The stem processes were identified by the absence of immunoreactivity for the myelin protein P_0 (Figs. 8*A*,*B*; 9*A*,*B*). The stem process of DRG neurons was strongly immunostained with SMI-32, as the nerve cell bodies (Fig. 8*A*), but these regions were stained much weakly with phosphorylated neurofilament antibody, SMI-31 (Fig. 9*A*). The phosphorylated neurofilament immunoreactivity was markedly more intense within the myelinated segments than within the stem process (Fig. 9*A*). In summary, the nonmyelinated stem process had a staining pattern similar to that of the cell body of DRG neurons, showing enrichment of immunoreactivity for nonphosphorylated neurofilaments, and weak immunoreactivity for extensively phosphorylated neurofilaments. In the sections we examined, all the axons exhibiting intense phosphorylated neurofilament immunoreactivity were associated with myelin protein immunoreactivity, indicating that the intensity of staining for phosphorylated neurofilaments increased abruptly within the myelinated internodes.

These observations were extended by electron microscopic immunocytochemistry on thin sections (around 100 nm in thickness). This technique minimized the concerns about the immunofluorescence data: the differences in antibody penetration and the influence of neurofilament number, density, spacing, or distribution (clustering or not) on immunofluorescence pattern. The staining pattern was consistent with that observed at the light microscopic level. The myelinated axons had a higher density of immunogold particles representing phosphorylated neurofilament (*P*[+]), than did the stem process, whereas densities of immunogold particles for total NF-H, the phosphorylation-independent neurofilaments (*P*[ind]), in the myelinated axon and stem process were not statistically different (Fig. 10*B*,*C*). To compare the relative abundance of phosphorylated neurofilament epitopes between stem process and myelinated axon, we used the ratio of gold particle densities (*P*[+]:*P*[ind]). Myelinated axons had relatively more phosphorylated epitopes than did the stem process, with about a 20-fold increase]*P*[+]:*P*[ind] = 2.1 ± 1.1 (mean ± SD) for myelinated internodes, and 0.1 ± 0.1 for stem processes, $p < 0.02$] (Fig. 10*D*).

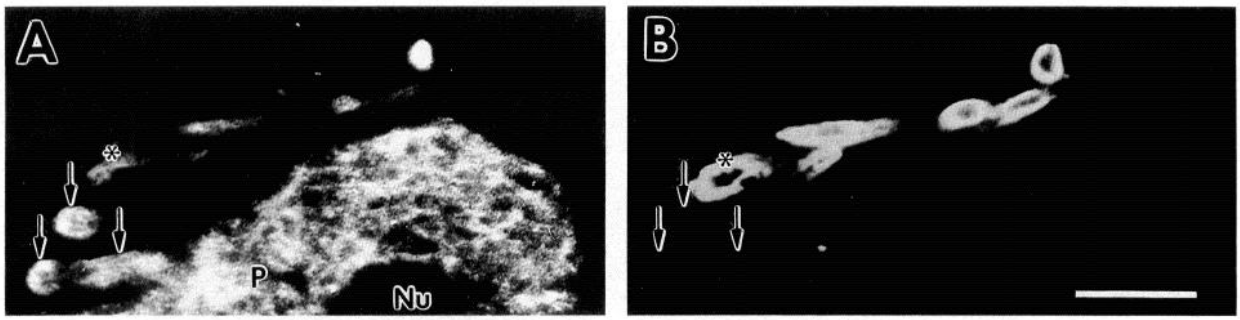

Figure 8. Immunofluorescence of dorsal root ganglion (DRG) neurons doubly labeled with antibodies against nonphosphorylated neurofilaments and myelin proteins. The DRG neurons were doubly immunostained with antibodies against nonphosphorylated neurofilaments, SMI-32 (*A*), and myelin protein, P_0 (*B*), simultaneously, and then subject to confocal laser scanning microscopy. Shown here was a 1 μm optical section through a portion of a DRG neuron with its stem process and myelinated axons. Due to the torturous course of the stem process, several profiles of stem process (*arrows* in *A*) would appear on the same section. Strong SMI-32 immunoreactivity was present in the perikaryon (*p*), but not in the nucleus (*Nu*). The stem process, which had a tortuous course (*arrows* in *A*), had the same staining pattern for nonphosphorylated neurofilaments as the perikaryon. P_0 antiserum labeled the myelin sheaths of several myelinated axonal profiles, one of which was marked with * in *B*. The stem processes were unstained with P_0 (*arrows* in *B*). The myelinated axons, one of which was marked with * in *A*, were also stained with the antibody against nonphosphorylated neurofilaments. Scale bar, 10 μm.

Discussion

Compared to the cell bodies, the nonmyelinated stem processes and the nodes of Ranvier, the axonal cytoskeleton in myelinated segments is modified in at least three regards: (1) the level of phosphorylation of NF-H is higher, (2) the spacing between neurofilaments is greater, and (3) there are more neurofilaments. These correlates of myelination are local, and recent results indicate that the first two can be reversed by demyelination (de Waegh et al., 1992), suggesting that they are effects of myelination. All of these correlates of myelination have the effect of increasing the size of myelinated segments, as discussed below. Taken together they suggest that the regulation of axonal caliber is influenced by mutual local interactions between the axon and the Schwann cell, as well as by developmental and target-derived influences on the whole neuron.

Myelination correlates with neurofilament phosphorylation and spacing

Previous studies have found low levels of phosphorylated neurofilament immunoreactivity in the perikarya, dendrites, and short initial segments, and usually have found that phosphorylation is high within the axons (Sternberger and Sternberger, 1983; Lee et al., 1986, 1987; Oblinger, 1987). Because the initial segment is very short in the neurons, it was not clear whether increased phosphorylation is an intrinsic feature of axon per se, or whether it is influenced by the presence of the myelination. By the combination of double labeling immunofluorescence and confocal laser microscopy, we were able to follow and reconstruct the nonmyelinated stem process of primary sensory neurons and found that intense phosphorylated neurofilament immunoreactivity always appeared with acquisition of myelin sheath; in the stem process, nonphosphorylated epitopes predominated. Mata et al. (1992) found low phosphorylated neurofilament immunoreactivity in the node of Ranvier of the rat sciatic nerve, suggesting that this same pattern is found wherever the axon is not covered by a myelin sheath. These results suggest that neurofilaments are in a low phosphorylation state as they are transported through the cell body and down the stem process, and become heavily phosphorylated in the myelinated internodes.

Not only is neurofilament phosphorylation higher in myelinated segments, but neurofilament spacing is greater. Taken together, these data suggest that myelination changes the interfilament spacing by altering local neurofilament phosphorylation and consequently the extent of negative charges on the side arms (Carden et al., 1987). Our data suggest that spacing increases directly with the thickness of the myelin sheath, so that the thicker the sheath the greater the spacing. Mean filament spacing correlated both with axonal caliber and myelin sheath thickness,

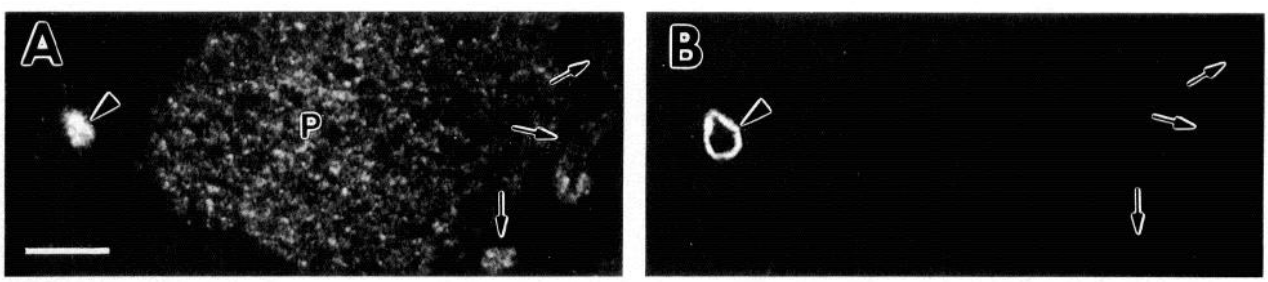

Figure 9. Immunofluorescence of dorsal root ganglion (DRG) neurons doubly labeled with antibodies against phosphorylated neurofilaments and myelin proteins. The DRG neurons were simultaneously stained with antibodies against phosphorylated neurofilaments, SMI-31 (*A*), and myelin protein, P_0 (*B*), and scanned by confocal laser microscopy. This 1 μm optical section demonstrated a portion of the DRG neuron with its perikaryon (*p*), and three profiles of the stem process, recognized by the absence of P_0 staining (*arrows* in *A* and *B*). The immunoreactivity for SMI-31 was barely detectable or appeared as weakly stained punctate dots in the perikaryon (*p*) and stem process (*arrows* in *A*), while staining was intense and homogenous in the myelinated internodes (*arrowheads* in *A* and *B*). Scale bar, 10 μm

but the higher correlation coefficient suggested that thickness of the myelin sheath was the major influence.

The effect of myelination on neurofilament phosphorylation and spacing is local and reversible, as demonstrated by de Waegh et al., (1992). In the *Trembler* mouse the demyelinated internodes were smaller and neurofilaments were less phosphorylated and more closely spaced than in control mice. The molecular defect in the *Trembler*, a point mutation affecting the myelin protein PMP-22 (Suter et al., 1992), indicates that abnormality is in the Schwann cell rather than the axon. To further examine the effect of myelinating Schwann cells on neurofilament organization, experiments employing tellurium-induced demyelinating neuropathy indicated that neurofilament spacing in the remyelinating axons was increased compared with the demyelinated axons (Hsieh et al., 1993).

Effects of myelination on neurofilament number

Neurofilaments have been proposed to be the major intrinsic determinant of axonal caliber (Hoffman et al., 1987). Their number and their spacing could each separately affect axonal caliber. The present study suggests that myelination increases both number and spacing. Increased neurofilament spacing accounts for about 25–50% of the difference in caliber between the nodes/stem process and the myelinated segments. The total number of microtubules remains the same in all of these regions. The remainder, up to 75% of the difference, is accounted for by the greater total number of neurofilaments in the myelinated segments. This is consistent with the previous reports indicating that myelinated internodes have more neurofilaments than the nodes of Ranvier (Price et al., 1990; Reles and Friede, 1991).

How myelination might affect neurofilament number in the myelinated segments is unclear. One possibility is that phosphorylation, by influencing the interactions between neurofilaments, might slow the transport of neurofilaments locally in the myelinated internodes. Increased phosphorylation has been associated with slowed transport in some reports (Watson et al., 1989a,b, 1991; Archer et al., 1994) but not all (de Waegh et al., 1992), and focal slowing could lead to accumulations of neurofilaments as argued by Hoffman et al. (1985). Another possibility is that phosphorylation alters the proportion of neurofilaments that are undergoing proximodistal transport. Whether most neurofilament organelles are moving (Lasek et al., 1992) or most are stationary has been a controversial issue (for reviews, see Hollenbeck, 1989; Lasek et al., 1992; Ochs and Brimijoin, 1993). Several lines of evidence suggest that there is a substantial stationary cytoskeleton (Nixon and Logvinenko, 1986; Nixon et al., 1987; Hollenbeck, 1989; Nixon and Sihag, 1991), and that phosphorylated neurofilaments are closely associated with the stationary phase (Watson et al., 1989a, 1991). Thus, by increasing phosphorylation locally, myelination might encourage local retention of neurofilaments as part of the stationary cytoskeleton. A final possibility is that myelination encourages local assembly of neurofilaments from subunits and precursors (Angelides et al., 1989; Okabe et al., 1993). In any event, although demyelination reverses the phosphorylation of neurofilaments in the underlying axons, it has a lesser effect on neurofilament number (de Waegh et al., 1992).

Conclusions

The axon dictates whether or not the Schwann cell forms myelin, and survival of the myelin sheath usually requires continued axonal innervation of the Schwann cell (for review, see Bunge and Griffin, 1992; Griffin et al., 1993). These facts have contributed to an axocentric view of axon–Schwann cell interactions. The present data, in combination with other recent observations (Windebank et al., 1985; de Waegh et al., 1992), show

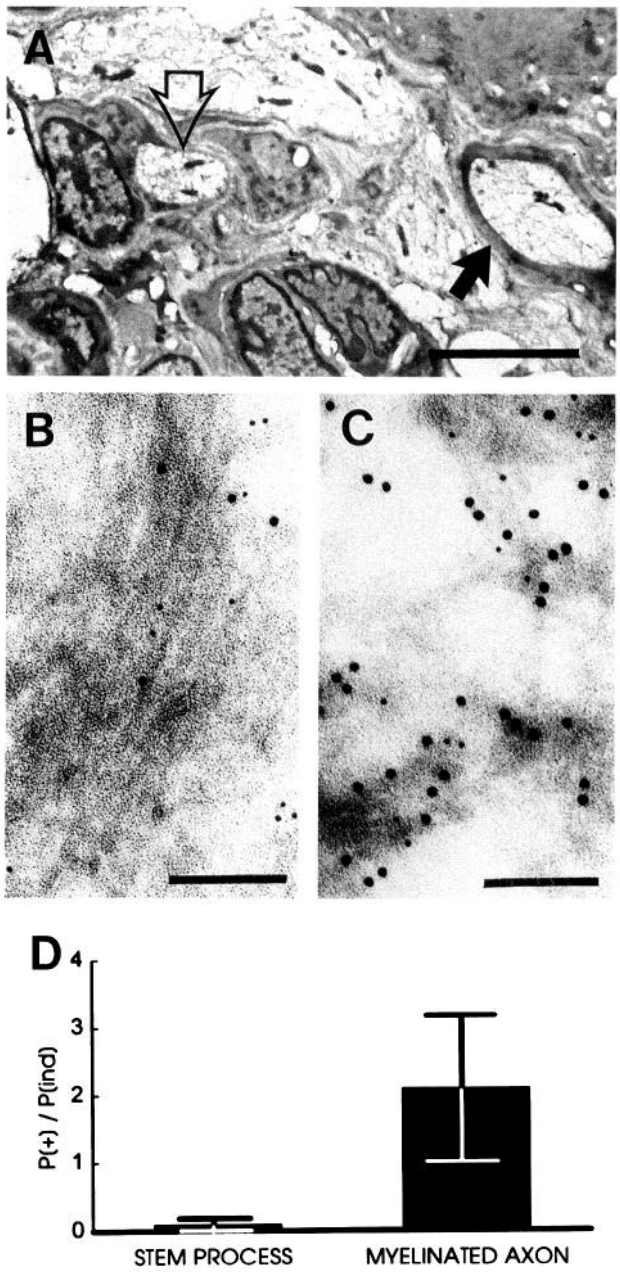

Figure 10. Immunogold labeling of different neurofilament epitopes in the stem process and myelinated axon of dorsal root ganglion (DRG) neurons. In electron microscopic immunocytochemistry (as described in Materials and Methods), the antibody against phosphorylated neurofilaments (*P*[+] for SMI-31), was labeled with 10 nm gold particles, while the antibody against total neurofilaments (the phosphorylation-independent antibody, *P*[ind] for pAb-NFH), was labeled with 5 nm gold particles. For each DRG neuron, the stem process (*open arrow* in *A*) as well as the myelinated axon (*solid arrow* in *A*) were selected and gold particles were counted. In the stem process (*B*), densities of 10 nm gold particles for *P*[+] were much lower than those in myelinated axons (*C*). When the relative extent of neurofilament phosphorylation was expressed as the ratio of gold particle densities, *P*[+]:*P*[ind], myelinated axons ($n = 5$) had the higher ratio than stem process ($n = 5$) [2.1 ± 1.1 vs 0.1 ± 0.1 (mean $\pm$ SD), $p < 0.02$ by Wilcoxon rank sums test] (*D*). Scale bars: *A*, 5 μm; *B* and *C*, 100 nm.

that the local axonal phenotype is profoundly modified by the ensheathing Schwann cell, necessitating a reappraisal of the relative roles of the axon and the Schwann cell in their interactions. Understanding the mechanism of this Schwann cell–axon interaction has implications for developmental neurobiology and for demyelinating diseases.

References

Aguayo AJ, Attiwell M, Trecarten J, Perkins S, Bray GM (1977) Abnormal myelination in transplanted *Trembler* mouse Schwann cells. Nature 265:73–75.

Angelides KJ, Smith KE, Takeda M (1989) Assembly and exchange of intermediate filament proteins of neurons: neurofilaments are dynamic structures. J Cell Biol 108:1495–1506.

Archer DA, Watson DF, Griffin JW (1994) Phosphorylation-dependent immunoreactivity of neurofilaments and the rate of slow axonal transport in the central and peripheral axons of the rat dorsal root ganglion. J Neurochem, in press.

Berthold C-H (1978) Morphology of normal peripheral axons. In: Physiology and pathobiology of axons (Waxman SG, ed), pp 3–63. New York: Raven.

Bunge RP, Griffin JW (1992) The cell of Schwann. In: Diseases of the nervous system, clinical neurobiology (Asbury AK, McKhann GM, McDonald WI, eds), pp 87–100. Philadelphia: Saunders.

Carden MJ, Schlaepfer WW, Lee VM-Y (1985) The structure, biochemical properties, and immunogenicity of neurofilament peripheral regions are determined by phosphorylation state. J Biol Chem 260: 9805–9817.

Carden MJ, Trojanowski JQ, Schlaepfer WW, Lee VM (1987) Two-stage expression of neurofilament polypeptides during rat neurogenesis with early establishment of adult phosphorylation patterns. J Neurosci 7:3489–3504.

de Waegh S, Brady ST (1990) Altered slow transport and regeneration in a myelin-deficient mutant mouse: the *Trembler* as an *in vivo* model for Schwann–axon interactions. J Neurosci 10:1855–1865.

de Waegh SM, Brady ST (1991) Local control of axonal properties by Schwann cells: neurofilaments and axonal transport in homologous and heterologous nerve grafts. J Neurosci Res 30:201–212.

de Waegh SM, Lee VM, Brady ST (1992) Local modulation of neurofilament phosphorylation, axonal caliber, and slow axonal transport by myelinating Schwann cells. Cell 68:451–463.

Dyck PJ, Lais AC, Giannini C, Engelstad JK (1990) Structural alterations of nerve during cuff compression. Proc Natl Acad Sci USA 87: 9828–9832.

Friede RL, Samorajski T (1970) Axon caliber related to neurofilaments and microtubules in sciatic nerve fibers of rats and mice. Anat Rec 167:379–388.

Geisler N, Kaufmann E, Fischer S, Plessmann U, Weber K (1983) Neurofilament architecture combines structural principles of intermediate filaments with carboxy-terminal extensions increasing in size between triplet proteins. EMBO J 2:1295–1302.

Griffin JW, Kidd G, Trapp BD (1993) Interactions between axons and Schwann cells. In: Peripheral neuropathy (Dyck PJ, Thomas PK, Griffin JW, Low PA, Poduslo JF, eds), pp 317–330. Philadelphia: Saunders.

Hirokawa N, Glicksman MA, Willard MB (1984) Organization of mammalian neurofilament polypeptides within the neuronal cytoskeleton. J Cell Biol 98:1523–1536.

Hisanaga S, Hirokawa N (1988) Structure of peripheral domains of neurofilaments revealed by low angle rotary shadowing. J Mol Biol 202:297–305.

Hoffman PN, Lasek RJ (1975) The slow component of axonal transport: identification of major structural polypeptides of axon and their generality among mammalian neurons. J Cell Biol 66:351–366.

Hoffman PN, Griffin JW, Price DL (1984) Control of axonal caliber by neurofilament transport. J Cell Biol 99:705–714.

Hoffman PN, Griffin JW, Gold BG, Price DL (1985) Slowing of neurofilament transport and the radial growth of developing nerve fibers. J Neurosci 5:2920–2929.

Hoffman PN, Cleveland DW, Griffin JW, Landes PW, Cowan NJ, Price DL (1987) Neurofilament gene expression: a major determinant of axonal caliber. Proc Natl Acad Sci USA 84:3472–3476.

Hollenbeck PJ (1989) The transport and assembly of axonal cytoskeleton. J Cell Biol 108:223–227.

Hsieh S-T, Crawford TO, Bouldin TW, Griffin JW (1993) Influence of demyelination and remyelination on axonal organization. Brain Pathol 3:307.

Hsieh S-T, Crawford TO, Griffin JW (1994) Neurofilament distribution and organization in the myelinated axons of the peripheral nervous system. Brain Res, in press.

Julien J-P, Mushynski WE (1983) The distribution of phosphorylation sites among identified proteolytic fragments of mammalian neurofilaments. J Biol Chem 258:4019–4025.

Julien J-P, Meyer D, Flavell D, Hurst J, Grosveld F (1986) Cloning and developmental expression of the murine neurofilament gene family. Mol Brain Res 1:243–250.

Julien J-P, Cote F, Beaudet L, Sidky M, Flavell D, Grosveld F, Mushynski W (1988) Sequence and structure of the mouse gene coding for the largest neurofilament subunit. Gene 68:307–314.

Laemmli UK (1970) Cleavage of structural proteins during the assembly of the head of bacteriophage T4. Nature 227:680–685.

Lasek RJ (1988) Studying the intrinsic determinants of neuronal form and function. In: Intrinsic determinants of neuronal form and function (Lasek RJ, Black MM, eds), pp 1–60. New York: Liss.

Lasek RJ, Paggi P, Katz MJ (1992) Slow axonal transport mechanisms move neurofilaments relentlessly in mouse optic axons. J Cell Biol 117:607–616.

Lee VM-Y, Carden MJ, Trojanowski JQ (1986) Novel monoclonal antibodies provide evidence for the *in situ* existence of a nonphosphorylated form of the largest neurofilament subunit. J Neurosci 6:850–858.

Lee VM-Y, Carden MJ, Schlaepfer WW, Trojanowski JQ (1987) Monoclonal antibodies distinguish several differentially phosphorylated states of the two largest rat neurofilament subunits (NF-H and NF-M) and demonstrate their existence in the normal nervous system of adult rats. J Neurosci 7:3474–3488.

Lee VM-Y, Otvos L Jr, Carden MJ, Hollosi M, Dietzschold B, Lazzarini RA (1988) Identification of the major multiphosphorylation site in mammalian neurofilaments. Proc Natl Acad Sci USA 85:1998–2002.

Lees JF, Shneidman PS, Skuntz SF, Carden MJ, Lazzarini RA (1988) The structure and organization of the human heavy neurofilament subunit (NF-H) and the gene encoding it. EMBO J 7:1947–1955.

Liem RKH, Yen S-H, Salomon GD, Shelanski ML (1978) Intermediate filaments in nervous tissues. J Cell Biol 79:637–645.

Lopata MA, Cleveland DW (1987) In vivo microtubules are copolymers of available β tubulin isotypes: localization of each of six vertebrate β tubulin isotypes using polyclonal antibodies elicited by synthetic peptide antigens. J Cell Biol 105:1707–1720.

Mata M, Kupina N, Fink DJ (1992) Phosphorylation-dependent neurofilament epitopes are reduced at the node of Ranvier. J Neurocytol 21:199–210.

Nixon RA, Logvinenko KB (1986) Multiple fates of newly synthesized neurofilament proteins: evidence for a stationary neurofilament network distributed nonuniformly along axons of retinal ganglion cell neurons. J Cell Biol 102:647–659.

Nixon RA, Sihag RK (1991) Neurofilament phosphorylation: a new look at regulation and function. Trends Neurosci 14:501–506.

Nixon RA, Lewis SE, Marotta CA (1987) Posttranslational modification of neurofilament proteins by phosphate during axoplasmic transport in retinal ganglion cell neurons. J Neurosci 7:1145–1158.

Oblinger MM (1987) Characterization of posttranslational processing of the mammalian high-molecular-weight neurofilament protein *in vivo*. J Neurosci 7:2510–2521.

Ochs S, Brimijoin WB (1993) Axonal transport. In: Peripheral neuropathy (Dyck PJ, Thomas PK, Griffin JW, Low PA, Poduslo JF, eds), pp 331–360. Philadelphia: Saunders.

Okabe S, Miyasaka H, Hirokawa N (1993) Dynamics of the neuronal intermediate filaments. J Cell Biol 121:375–386.

Parhad IM, Clark AW, Griffin JW (1987) Effect of changes in neurofilament content on caliber of small axons: the β,β'-iminodipropionitrile model. J Neurosci 7:2256–2263.

Price RL, Lasek RJ, Katz MJ (1990) Internal axonal cytoarchitecture is shaped locally by external compressive forces. Brain Res 530:205–214.

Reles A, Friede RL (1991) Axonal cytoskeleton at the nodes of Ranvier. J Neurocytol 20:450–458.

Schlaepfer WW (1987) Neurofilaments: structure, metabolism and implications in disease. J Neuropathol Exp Neurol 46:117–129.

Spencer PS, Raine CS, Wisniewski H (1973) Axonal diameter and

myelin thickness—unusual relationships in dorsal root ganglia. Anat Rec 176:225–244.

Sternberger LA, Sternberger NH (1983) Monoclonal antibodies distinguish phosphorylated and nonphosphorylated forms of neurofilaments *in situ*. Proc Natl Acad Sci USA 80:6126–6130.

Suter U, Welcher AA, Ozcelik T, Snipes GJ, Kosaras B, Francke U, Billings-Gagliardi S, Sidman RL, Shooter EM (1992) *Trembler* mouse carries a point mutation in a myelin gene. Nature 356:241–244.

Thomas PK, Ochoa J (1984) Microscopic anatomy of peripheral nerve fibers. In: Peripheral neuropathy (Dyck PJ, Thomas PK, Lambert EH, Bunge R, eds), pp 39–96. Philadelphia: Saunders.

Trapp BD, Itoyama Y, Sternberger NH, Quarles RH, Webster HdeF (1981) Immunocytochemical localization of P_0 protein in Golgi complex membranes and myelin of developing rat Schwann cells. J Cell Biol 90:1–6.

Trapp BD, Andrews SB, Wong A, O'Connell M, Griffin JW (1989) Co-localization of myelin-associated glycoprotein and the microfilament components, F-actin and spectrin, in Schwann cells of myelinated nerve fibers. J Neurocytol 18:47–60.

Watson DF, Griffin JW, Fittro KP, Hoffman PN (1989a) Phosphorylation-dependent immunoreactivity of neurofilaments increases during axonal maturation and β,β'-iminodipropionitrile intoxication. J Neurochem 53:1818–1829.

Watson DF, Hoffman PN, Fittro KP, Griffin JW (1989b) Neurofilament and tubulin transport slows along the course of mature motor axons. Brain Res 477:225–232.

Watson DF, Fittro KP, Hoffman PN, Griffin JW (1991) Phosphorylation-related immunoreactivity and the rate of transport of neurofilaments in chronic 2,5-hexanedione intoxication. Brain Res 539: 103–109.

Waxman SG (1980) Determinants of conduction velocity in myelinated nerve fibers. Muscle Nerve 3:141–150.

Willard M, Simon C (1983) Modulations of neurofilament axonal transport during the development of rabbit retinal ganglion cells. Cell 35:551–559.

Windebank AJ, Wood P, Bunge RP, Dyck PJ (1985) Myelination determines the caliber of dorsal root ganglion neurons in culture. J Neurosci 5:1563–1569.